Journal of Industrial and Engineering Chemistry 65 (2018) 175–179

Contents lists available at ScienceDirect

Journal of Industrial and Engineering Chemistry

journal homepage: www.elsevier.com/locate/jiec

Organic electrolyte hybridized ZnO as the electron transport layer for inverted polymer solar cells

Dong Geun Kim[a], Youn Hwan Kim[a], Ratna Dewi Maduwu[a], Ho Cheol Jin[a], Doo Kyung Moon[b], Joo Hyun Kim[a,*]

[a] Department of Polymer Engineering, Pukyong National University, Busan 48547, Republic of Korea
[b] Department of Materials Chemistry and Engineering, Konkuk University, Seoul 05029, Republic of Korea

ARTICLE INFO

Article history:
Received 14 February 2018
Received in revised form 9 April 2018
Accepted 20 April 2018
Available online 27 April 2018

Keywords:
Electrolyte
Doping
Electron transporting layer
Inverted polymer solar cell

ABSTRACT

Small molecular organic electrolyte; *N*,*N*,*N*,*N*,*N*,*N*-hexakis(2-hydroxyethyl)butane-1,4-diaminium bromide (**C4**), doped ZnO is prepared by a typical sol–gel process and used as the for an electron transport layer in inverted polymer solar cells (PSCs). The electron mobility of the doped ZnO is comparable to that of pristine ZnO because the crystallinity of the ZnO layer is not significantly affected by the doping process. The Kelvin probe microscopy measurements employ that the work function of doped ZnO are −4.0 eV, which is higher than that of pristine ZnO (−4.5 eV). This is due to that the formation of interface dipole at the interface between the ZnO layer and the active layer by unreacted hydroxyl groups and quaternary ammonium bromide. As a result, inverted PSC based on **C4** doped ZnO exhibit the power conversion efficiency (PCE) up to 8.87%, which is a significant improvement over the device based on pristine ZnO (PCE = 7.4%). Note that the main contribution to the enhancement of the PCE is from the improvement of the J_{sc}.

Introduction

Due to their many advantages such as low fabrication cost, light weight, large area application, and flexible devices [1–3], polymer solar cells (PSCs) have attracted greatly interests. There have been a rapid growth in the power conversion efficiencies (PCEs) of PSCs by tremendous innovative efforts, including synthesis of new materials [4–6] and device optimization [7]. Recently 10% of PCES or more have been reported continuously [8–10].

In conventional type PSCs, poly(3,4-ethylenedioxythiophene): poly(styrenesulfonate) (PEDOT:PSS) deteriorates the ITO electrode due to its highly acidic nature. Inverted type PSCs have been proposed because of their better stability than the conventional architecture [11–15]. A ZnO layer prepared by a sol–gel process is widely used as the electron transport layer between the ITO cathode and the active layer [16]. As for inverted PSCs, one of the crucial factors to improve the PCE is the efficient electron collection at the interface between the ZnO layer and the photoactive layer. Therefore, making an ohmic contact at the cathode interface and passivation of the ZnO layer are very important. Many efforts, such as deposition of thin layer of conjugated or non-conjugated polyelectrolytes [17–26] (i.e. interlayer) and self-assembled monolayer (SAM) [27–30] treatments on top of the ZnO surface have been applied to improve electron collection capability of at the ZnO layer. In the case of an applied interlayer, device performance is very sensitive to the thickness of the interlayer, which is normally in the range of 5–10 nm and should be optimized. However, it is very difficult to control the interlayer thickness in the range of 5–10 nm using the large area fabrication systems seen in the practical applications, such as spray coating or slot die casting processes. Thus, an alternative method, which avoids the need for fine control of interlayer thickness, is to blend polymers or small molecules, such as poly(ethyleneoxide) [27], polyethyleneimine [28], and C60 derivatives [29] into a ZnO matrix. Devices based on blended ZnO showed improved performance. However, the electron transporting property (i.e. electron mobility) of such blended ZnO layers were decreased because of the intrinsically insulating nature of the polymers. To overcome this problem, blends of ZnO with small molecules, such as 1,2-ethanedithiol [30] and ethylenediaminetetraacetic acid (EDTA) [31] have been used as electron transporting layer.

In this report, we describe the preparation of *N*,*N*,*N*,*N*,*N*,*N*-hexakis(2-hydroxyethyl)butane-1,4-diaminium bromide (**C4**) [23]

* Corresponding author.
E-mail address: jkim@pknu.ac.kr (J.H. Kim).

https://doi.org/10.1016/j.jiec.2018.04.026
1226-086X/

doped ZnO layers and their use as electron transporting layers in inverted type PSCs in order to device performances without sacrificing electron mobility. As shown in Fig. 1, **C4** doped ZnO layers can be prepared by a typical sol–gel process. Homogeneous ZnO layer can be produced due to multiple hydroxyl (—OH) groups in **C4**. Doping of **C4** in the ZnO matrix improves the PCE from 7.4% (short circuit current (J_{sc}) = 14.7 mA/cm^2, open circuit voltage (V_{oc}) = 0.76 V, fill factor (FF) = 66.6%) based on pristine ZnO to 8.87% (J_{sc} = 17.1 mA/cm^2, V_{oc} = 0.74 V, FF = 70.0%) at a doping concentration of 3.0 wt.% versus $Zn(OAc)_2$, without sacrificing the electron mobility of the ZnO layer. Improvement in the PCE of the devices results mainly from the enhanced J_{sc}. This is due to the improvement in the collectron collection capability from the active layer to the electron transport layer by reducing the energy barrier at the cathode interface.

Results and discussion

*Characterization of **C4** doped ZnO*

We used X-ray photoelectron spectroscopy (XPS) to characterize **C4** doped ZnO layers. Fig. 2(a) shows the survey spectra of pristine ZnO and 3.0 wt.% **C4** doped ZnO. Peaks corresponding to both nitrogen and bromide appeared in the survey spectrum of the 3.0 wt.% **C4** doped ZnO sample, whereas, both peaks from these elements not appeared in the survey spectrum of pristine ZnO. Peaks at binding energies (BEs) of 401, 252, 185, 178, and 65 eV correspond to N1s, Br3d, Br3p3/2, Br3p1/2, and Br3s, respectively. From the survey spectra, we confirmed the existence of **C4** in the ZnO layer. Peaks at BE of 1045 and 1021 eV (Fig. 2(b)) correspond to Zn 2p1/2 and Zn 2p3/2, respectively [16]. The position of both peaks from ZnO with **C4** are shifted toward higher energy than those peaks from pristine ZnO [32,33]. This is due the change in the surroundings of the Zn atoms, which has become more electron rich compared to undoped ZnO sample. The more electron rich state near the Zn atoms is consistent with the formation of chemical bonds between Zn and **C4**. As shown in the XPS spectra of pristine ZnO and **C4** doped ZnO (Fig. 2(c)), peaks at BEs of 532 and 530 eV are assigned to oxygen ions in —OH groups in/ZnO, respectively. The peak intensities of O-H/Zn-O from **C4** doped ZnO is higher than that of pristine ZnO. Apparently, the number of defect sites in the **C4** doped ZnO layer is greater than in the pristine ZnO layer. However, the number of defect sites cannot be estimated from the XPS results because the peak intensity at a BE of 532 eV originates from both the oxygen defects in ZnO and free —OH groups in **C4**.

To further investigate the existence of defect sites in ZnO layers, we measured the photoluminescence (PL) spectra of the ZnO layers. As shown in Fig. 3(a), the emission band at 383 nm is assigned to the band-edge emission. In addition a very weak emission band at 510 nm was observed, which corresponds to the

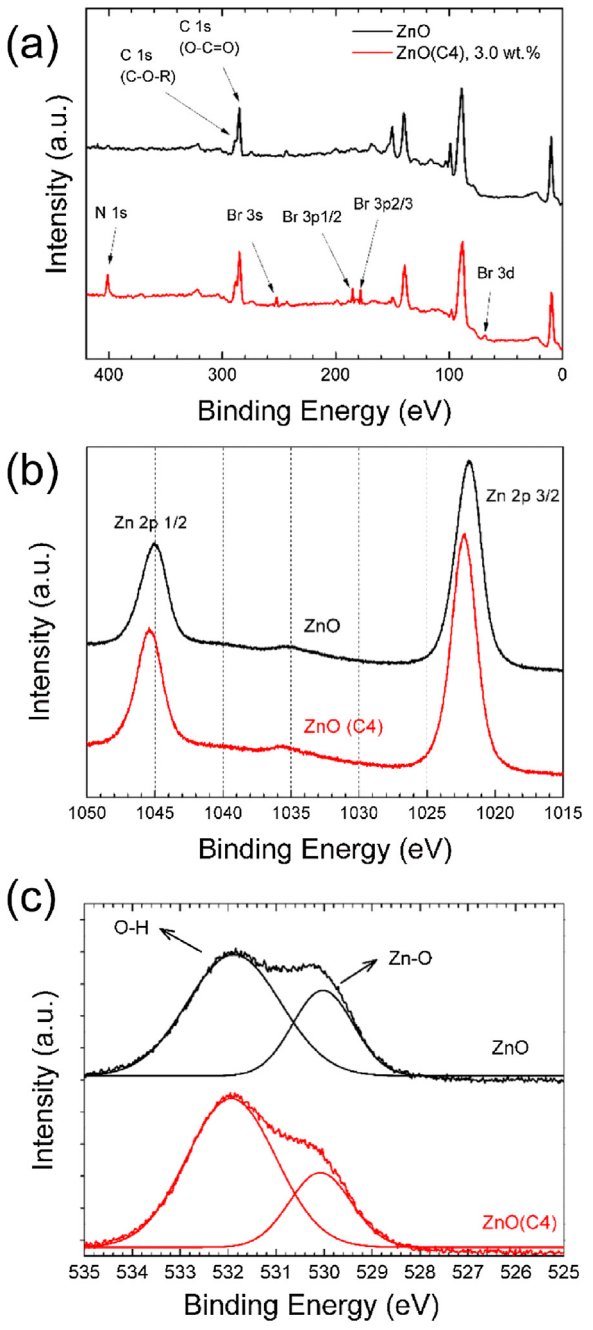

Fig. 2. (a) XPS survey spectra, (b) Zn 2p, and (c) O 1s spectra of pristine ZnO and 3.0 wt.% **C4** doped ZnO.

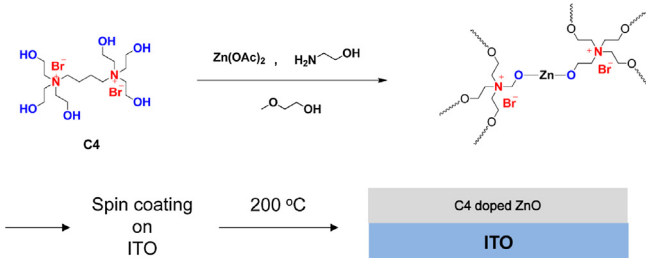

Fig. 1. Chemical structure of **C4** and schematic illustration of preparation of **C4** doped ZnO layer.

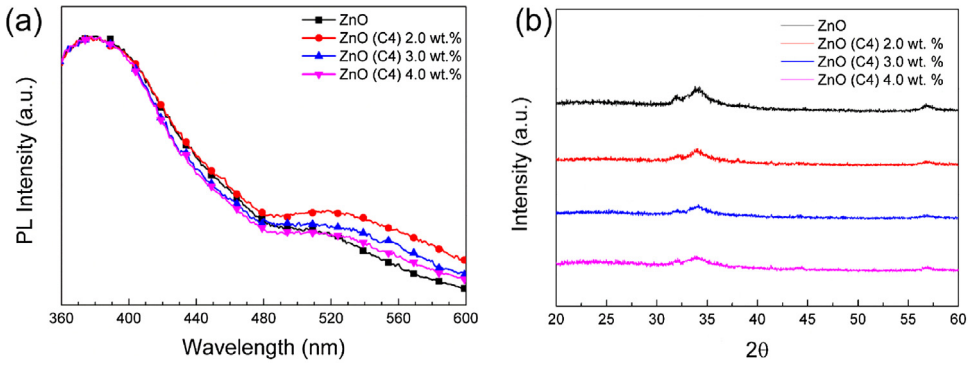

Fig. 3. Normalized PL spectra of pristine ZnO and **C4** doped ZnO. (Excited at 325 nm).

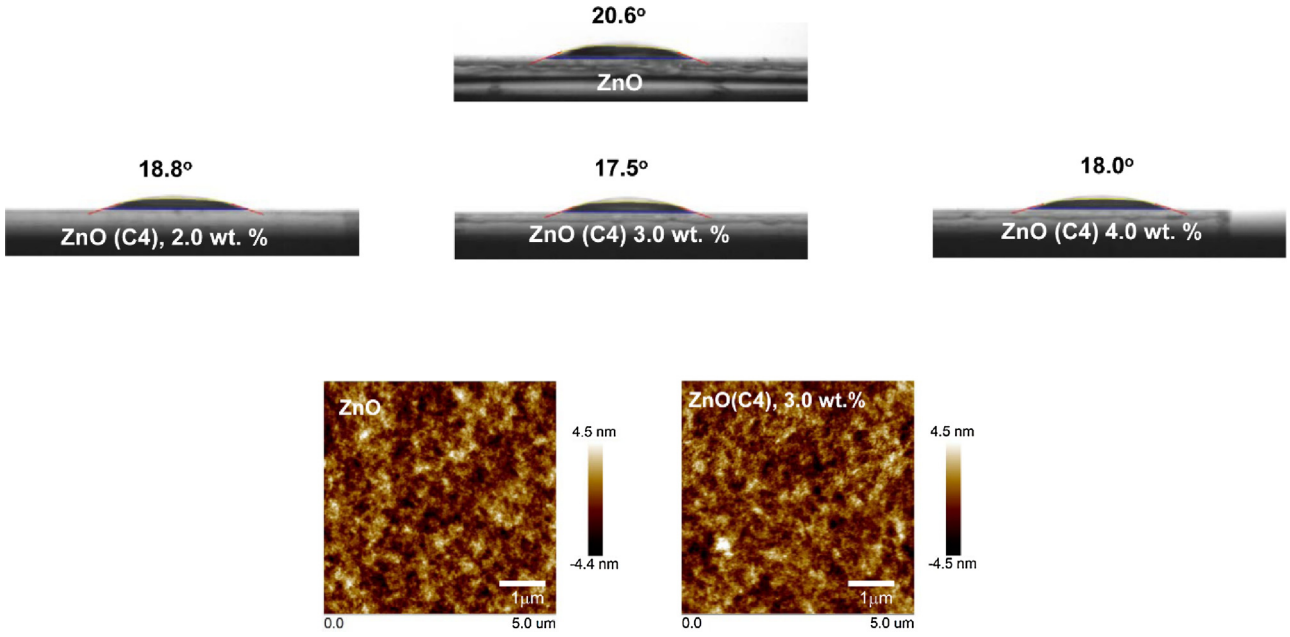

Fig. 4. Static water contact angle data and AFM images of ZnO and **C4** doped ZnO.

defect sites. The intensity of the band at 510 nm for the **C4** doped ZnO is slightly higher than for the pristine ZnO. In addition, the emission corresponding to defect sites slightly deteriorated with increasing concentration of C4 up to 4.0 wt.%. However, one can notice that the doping process does not significantly affect the generation of defect sites. X-ray diffraction (XRD) patterns also provide evidence of the existence of defect sites. As can be seen in Fig. 3(b), both the pristine ZnO and **C4** doped ZnO layers showed relatively weak diffraction peaks because the annealing temperature was relatively low (200 °C). However, intensity of the peaks in **C4** doped ZnO layer are comparable to those of the pristine ZnO film. This means that the addition of **C4** up to 4.0 wt.% does not affect the crystallinity of ZnO. We investigated the static water contact angle (SWCA) and the surface morphology to investigate the surface properties of the ZnO layers (Fig. 4). The SWCA of the surface of **C4** doped ZnO was smaller than that of the pristine ZnO surface, indicating that the surface of **C4** doped ZnO becomes more hydrophilic than the surface of pristine ZnO. This is due to the unreacted free hydroxyl groups in **C4**. These results are consistent with the PL results. The surface roughness of the ZnO and **C4** doped ZnO surface are 1.04 nm and 1.02 nm, respectively. In addition, the surface morphology (Fig. 4) of the **C4** doped ZnO surface is almost identical to that of the pristine ZnO.

Photovoltaic properties

We fabricated a device based on **C4** doped ZnO as the electron transport layer with the structure of ITO/**C4** doped ZnO/PTB7:$PC_{71}BM$(1:1.5)/MoO_3/Ag to investigate the effect of **C4** doping on the photovoltaic properties. We prepared **C4** doped ZnO through the typical sol–gel process. A precursor solution was prepared by the addition of different weight ratios of **C4** (0.0, 2.0, 3.0 and 4.0 wt.%) to the zinc acetate dihydrates to find the optimum concentration of **C4**. Details are described in the Supporting information. Fig. 5(a) and (b) display the chemical structures and energy level diagram of the materials used in this research. Fig. 5(c) shows the current density–voltage curves of PSCs under illumination (inset: under the dark condition). In addition, a summary of the performance of the devices is shown in Table 1. According to the thermogravimetric analysis (TGA) data (see Fig. S1), carried out under ambient air atmosphere, **C4** showed good thermal stability up to 244 °C, which is the point of 5% weight loss (T_d) of **C4**. Thus, **C4** should be stable up to the annealing temperature used for the ZnO layer (200 °C).

As shown in Table 1, the J_{sc} and FF of the devices based on **C4** doped ZnO were enhanced from 14.7 mA/cm^2 to 15.5–17.1 mA/cm^2, while the V_{oc} slightly decreased from 0.76 V to 0.73–0.74 V. Among the devices tested, the 3.0 wt.% **C4** doped device exhibited the best

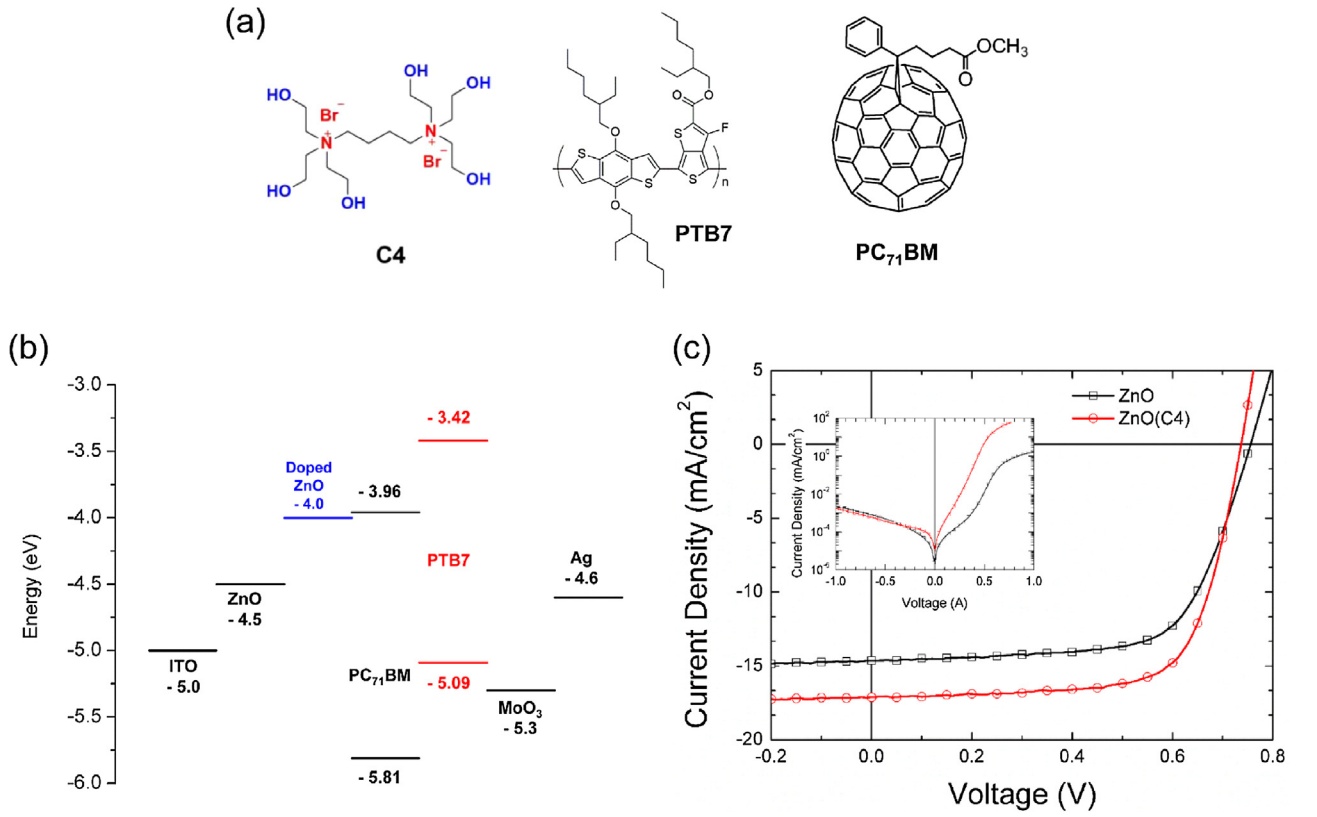

Fig. 5. (a) Structure of materials (b) energy level diagram of materials used inverted PSCs, and (c) current density–voltage curves of PSCs under illumination (inset: in the dark condition).

Table 1
Summary of the performances of PSCs having the best PCE. The averages and deviations (20 devices are averaged) are summarized in parentheses.

ETL	wt.%[a](mol.%)[b]	J_{sc} (mA/cm^2)	V_{oc} (V)	*FF* (%)	*PCE* (%)	R_s[c] (Ω cm^2)	Calculated J_{sc}[d] (mA/cm^2)
ZnO	0%	14.7 (14.36 ± 0.22)	0.76 (0.76 ± 0.01)	66.6 (67.8 ± 1.15)	7.41 (7.34 ± 0.10)	9.62	14.9
ZnO (**C4**)	2.0% (0.26%)	15.5 (15.29 ± 0.17)	0.74 (0.74 ± 0.00)	71.6 (71.0 ± 0.45)	8.20 (8.03 ± 0.12)	–	–
	3.0% (0.39%)	17.1 (16.30 ± 0.33)	0.74 (0.74 ± 0.00)	70.0 (70.6 ± 0.71)	8.87 (8.55 ± 0.14)	3.35	16.3
	4.0% (0.52%)	15.7 (15.52 ± 0.14)	0.73 (0.73 ± 0.00)	70.8 (70.8 ± 0.65)	8.12 (8.05 ± 0.05)	–	–

[a] Weight percent of **C4** to zinc acetate dihydrates.
[b] Mole percent of **C4** to zinc acetate dihydrates.
[c] Series resistance values are calculated from the device showing the best PCE.
[d] Calculated from the IPCE curve.

PCE of 8.87% with a J_{sc} of 17.1 mA/cm^2, a FF of 70.0%, and a V_{oc} of 0.74 V, which is a significant improvement over the device based on pristine ZnO. It should be noticed that the best PCE, obtained from the device with 3.0 wt.% of **C4**, mainly resulted from the improvement of the J_{sc}.

We investigated the work function of **C4** doped ZnO by Kelvin probe microscopy to verify these results. As shown in Fig. 5(b), the work function of **C4** with ZnO and pristine ZnO were −4.0 and −4.5 eV, respectively. The dopant concentration does not critically affected the work function of **C4** doped ZnO. However, the work function of a doped ZnO layer is higher than that of pristine ZnO. It should be noted that the J_{sc} result is strongly related to the work function of the electrodes. Charge collection behavior is strongly related to the barrier height at the electrode interface. Therefore, the J_{sc} enhancement is strongly correlated with the change in the work function of the ZnO layer.

Generally, the work function difference in the charge transporting layer is not main factor affecting the built-in potential and the V_{oc} in the case of Fermi-level pinning [34]. This is due to the fact that the V_{oc} of the device with **C4** is almost same as the device with pristine ZnO. The series resistances (R_s), as determined from the inverse slope near the high current regime in the dark current density–voltage curves, were 9.62 and 3.35 Ω cm^2 for of the device based on pristine ZnO and **C4** doped ZnO, respectively. The R_s data are well correlated with the performances of the devices. Incident photon-to-current efficiency (IPCE) curves (see Fig. S2) showed very good agreement with the J_{sc} data obtained from the devices.

As shown in the inset of Fig. 6, we fabricated electron-only devices to investigate the electron mobility of pristine ZnO and **C4** doped ZnO. The electron mobility of the devices were estimated using space-charge-limited current (SCLC) method and calculated using the Mott–Gurney equation [35,36]. As shown in Fig. 6, above built-in voltage, the current density and electric field showed the characteristics of SCLC. The electron mobility of the device with optimum concentration of **C4** doped ZnO was 8.83×10^{-4} cm^2 V^{-1} s^{-1}, which is very comparable to the electron mobility of pristine ZnO (7.58×10^{-4} cm^2 V^{-1} s^{-1}). This supports the fact that doping with **C4** improves the PCE of the device without sacrificing the electron mobility of the ZnO layer.

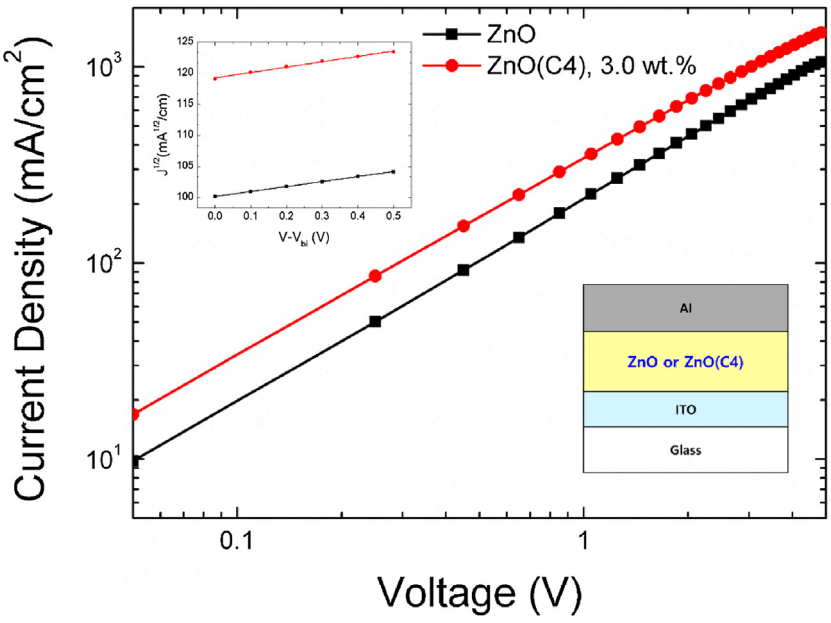

Fig. 6. Current density–voltage curves of electron-only device with fitted line (V, applied voltage; V_{bi}, built-in voltage).

Conclusion

Small molecular organic electrolyte (**C4**) doped ZnO have been successfully prepared. A ZnO layer with **C4** as a dopant improved the PCE from 7.4% (J_{sc} = 14.2 mA/cm^2, V_{oc} = 0.76 V, FF = 66.6%) based on pristine ZnO to 8.87% (J_{sc} = 17.1 mA/cm^2, V_{oc} = 0.74 V, FF = 70.0%) based on devicesusing **C4** doped ZnO without sacrificing the electron mobility of the ZnO layer. Improvement in the PCE of the devices is resulted from the J_{sc} improvement. This is due to the fact that the reduced energy barrier at the interface between the active layer and the electron transport layer allows for more efficient electron collection.

Acknowledgements

This research work was supported by the New & Renewable Energy Core Technology Program of the Korea Institute of Energy Technology Evaluation and Planning (KETEP) granted financial resource from the Ministry of Trade, Industry & Energy, Republic of Korea (20153010140030) and Basic Science Research Program through the National Research Foundation of Korea (NRF) funded by the Ministry of Education, Science and Technology (201603930154). D. G. Kim and Y. H. Kim contributed equally to this work

Appendix A. Supplementary data

Experimental details including materials, measurements, and fabrication of devices, TGA and IPCE data are available in Supporting information.

Supplementary data associated with this article can be found, in the online version, at https://doi.org/10.1016/j.jiec.2018.04.026.

References

[1] G. Yu, J. Gao, J.C. Hummelen, F. Wudl, A.J. Heeger, Science 270 (1995) 1789.
[2] S. Gunes, H. Neugebauer, N.S. Sariciftci, Chem. Rev. 107 (2007) 1324.
[3] L. Lu, T. Zheng, Q. Wu, A.M. Schneider, D. Zhao, L. Yu, Chem. Rev. 115 (2015) 12666.
[4] V. Vohra, K. Kawashima, T. Kakara, T. Koganezawa, I. Osaka, K. Takimiya, H. Murata, Nat. Photonics 9 (2015) 403.
[5] H.-J. Song, D.-H. Kim, E.-J. Lee, J.R. Hwa, D.-K. Moon, Sol. Energy Mater. Sol. Cells 123 (2014) 112.
[6] J. Zhao, Y. Li, G. Yang, K. Jiang, H. Lin, H. Ade, W. Ma, H. Yan, Nat. Energy 1 (2016) 15027.
[7] S.H. Oh, S.I. Na, J. Jo, B. Lim, D. Vak, D.Y. Kim, Adv. Funct. Mater. 20 (2010) 1977.
[8] Y.-J. Cheng, S.-H. Yang, C.-S. Hsu, Chem. Rev. 109 (2009) 5868.
[9] R. He, L. Yu, P. Cai, F. Peng, J. Xu, L. Ying, J. Chen, W. Yang, Y. Cao, Macromolecules 47 (2014) 2921.
[10] L. Huo, Z.A. Tan, X. Wang, Y. Zhou, M. Han, Y. Li, J. Polym. Sci. A: Polym Chem. 46 (2008) 4038.
[11] S. Nho, G. Baek, S. Park, B.R. Lee, M.J. Cha, D.C. Lim, J.H. Seo, S.-H. Oh, M.H. Song, S. Cho, Energy Environ. Sci. 9 (2016) 240.
[12] Y. Sun, J.H. Seo, C.J. Takacs, J. Seifter, A.J. Heeger, Adv. Mater. 23 (2011) 1679.
[13] H. Yan, P. Lee, N.R. Armstrong, A. Graham, G.A. Evmenenko, P. Dutta, T.J. Marks, J. Am. Chem. Soc. 127 (2005) 3172.
[14] K. Norrman, S.A. Gevorgyan, F.C. Krebs, ACS Appl. Mater. Interfaces 1 (2008) 102.
[15] M. Jørgensen, K. Norrman, S.A. Gevorgyan, T. Tromholt, B. Andreasen, F.C. Krebs, Adv. Mater. 24 (2012) 580.
[16] C.E. Small, S. Chen, J. Subbiah, C.M. Amb, S.-W. Tsang, T.-H. Lai, J.R. Reynolds, F. So, Nat. Photonics 6 (2012) 115.
[17] M.Y. Jo, Y.E. Ha, J.H. Kim, Sol. Energy Mater. Sol. Cells. 107 (2012) 1.
[18] M.Y. Jo, Y.E. Ha, J.H. Kim, Org. Electron. 14 (2013) 995.
[19] G.E. Lim, Y.E. Ha, M.Y. Jo, J. Park, Y.C. Kang, J.H. Kim, ACS Appl. Mater. Interfaces 5 (2013) 6508.
[20] Y.E. Ha, G.E. Lim, M.Y. Jo, J. Park, Y.C. Kang, S.J. Moon, J.H. Kim, J. Mater. Chem. C 2 (2004) 3820.
[21] W. Xu, Z. Kan, T. Ye, L. Zhao, W.-Y. Lai, R. Xia, G. Lanzani, P.E. Keivanidis, W. Huang, ACS Appl. Mater. Interfaces 7 (2015) 452.
[22] Y.H. Kim, N. Sylvianti, M.A. Marsya, J. Park, Y.-C. Kang, D.K. Moon, J.H. Kim, ACS Appl. Mater. Interfaces 8 (2016) 32992.
[23] Y.H. Kim, N. Sylvianti, M.A. Marsya, D.K. Moon, J.H. Kim, Org. Electron. 39 (2016) 163.
[24] T.T. Do, H.S. Hong, Y.E. Ha, S.I. Yoo, Y.S. Won, M.-J. Moon, J.H. Kim, Macromol. Res. 23 (2015) 367.
[25] J.P. Han, E.J. Lee, Y.W. Han, T.H. Lee, D.K. Moon, J. Ind. Eng. Chem. 45 (2017) 44.
[26] V.V. Duzhko, B. Dunham, S.J. Rosa, M.D. Cole, A. Paul, Z.A. Page, C. Dimitrakopoulos, T. Emrick, ACS Energy Lett. 2 (2017) 957.
[27] S. Shao, K. Zheng, T.N. Pullerits, F. Zhang, ACS Appl. Mater. Interfaces 5 (2013) 380.
[28] H.-C. Chen, S.-W. Lin, J.-M. Jiang, Y.-W. Su, K.-H. Wei, ACS Appl. Mater. Interfaces 7 (2015) 6273.
[29] S.-H. Liao, H.-J. Jhuo, Y.-C. Cheng, S.-A. Chen, Adv. Mater. 25 (2013) 4766.
[30] H. Yang, T. Wu, T. Hu, X. Hu, L. Chen, Y. Chen, J. Mater Chem. C 4 (2016) 8783.
[31] X. Li, X. Liu, W. Zhang, H.-Q. Wang, J. Fang, Chem. Mater. 29 (2017) 4176.
[32] D. Gao, J. Zhang, G. Yang, J. Zhang, Z. Shi, J. Qi, Z. Zhang, D. Xue, J. Phys. Chem. C 114 (2010) 13477.
[33] S.H. Liao, H.J. Jhuo, Y.S. Cheng, S.A. Chen, Adv. Mater. 25 (2013) 4766.
[34] E.L. Ratcliff, B. Zacher, N.R. Armstrong, J. Phys. Chem. Lett. 2 (2011) 1337.
[35] Y. Wang, Y. Liu, S. Chen, R. Peng, Z. Ge, Chem. Mater. 25 (2013) 3196.
[36] S. Guo, B. Cao, W. Wang, J.-F. Moulin, P. Muller-Buschbaum, ACS Appl. Mater. Interfaces 7 (2015) 4641.